UNIVERSITY OF HELSINKI REPORT SERIES IN PHYSICS

HU-P-D173

Irradiation of silicon particle detectors with MeV-protons

Samuli Väyrynen

Division of Materials Physics
Department of Physics
Faculty of Science
University of Helsinki
Helsinki, Finland

ACADEMIC DISSERTATION

To be presented, with the permission of the Faculty of Science of the University of Helsinki, for public criticism in the Auditorium D101 of the Department of Physics (Physicum), on 7 May, 2010, at 12 o'clock p.m.

HELSINKI 2010

ISBN 978-952-10-5975-9 (printed version)
ISSN 0356-0961
Helsinki 2010
Helsinki University Printing House (Yliopistopaino)

ISBN 978-952-10-5976-6 (PDF version)
http://ethesis.helsinki.fi/
Helsinki 2010
Electronic Publications @ University of Helsinki (Helsingin yliopiston verkkojulkaisut)

Samuli Väyrynen: **Irradiation of silicon particle detectors with MeV-protons**, 2010, 37 p.+appendices, University of Helsinki Report Series in Physics, HU-P-D173, ISSN 0356-0961, ISBN 978-952-10-5975-9 (printed version), ISBN 978-952-10-5976-6 (PDF version)

Classification (PACS): 07.90.+c, 61.82.Fk, 29.40.Wk, 85.30.De

Keywords: proton irradiation, silicon particle detector, current-voltage, capacitance-voltage

ABSTRACT

Silicon particle detectors are used in several applications and will clearly require better hardness against particle radiation in the future large scale experiments than can be provided today. To achieve this goal, more irradiation studies with defect generating bombarding particles are needed. Protons can be considered as important bombarding species, although neutrons and electrons are perhaps the most widely used particles in such irradiation studies. Protons provide unique possibilities, as their defect production rates are clearly higher than those of neutrons and electrons, and, their damage creation in silicon is most similar to the that of pions.

This thesis explores the development and testing of an irradiation facility that provides the cooling of the detector and on-line electrical characterisation, such as current-voltage (IV) and capacitance-voltage (CV) measurements. This irradiation facility, which employs a 5-MV tandem accelerator, appears to function well, but some disadvantageous limitations are related to MeV-proton irradiation of silicon particle detectors.

Typically, detectors are in non-operational mode during irradiation (i.e., without the applied bias voltage). However, in real experiments the detectors are biased; the ionising proton generates electron-hole pairs, and a rise in rate of proton flux may cause the detector to breakdown. This limits the proton flux for the irradiation of biased detectors. In this work, it is shown that, if detectors are irradiated and kept operational, the electric field decreases the introduction rate of negative space-charges and current-related damage.

The effects of various particles with different energies are scaled to each others by the non-ionising energy loss (NIEL) hypothesis. The type of defects induced by irradiation depends on the energy used, and this thesis also discusses the minimum proton energy required at which the NIEL-scaling is valid.

Contents

1 INTRODUCTION 4

2 PURPOSE AND STRUCTURE OF THE STUDY 6

2.1 List of articles 6

2.2 Author's contribution 7

3 SILICON PARTICLE DETECTOR 8

3.1 Operation principle of the detector 8

3.2 Diode-junction 9

3.2.1 Capacitance-voltage (CV) characteristics 10

3.2.2 Current-voltage (IV) characteristics 12

3.3 Avalanche breakdown 12

3.4 Processing of silicon particle detectors 14

4 IRRADIATION EFFECTS 16

4.1 Interaction processes 16

4.2 Bulk damage - non-ionising energy loss 17

4.2.1 Effects of defects on detector properties 18

4.2.2 NIEL scaling hypothesis 20

4.3 Ionising energy loss 21

4.3.1 Surface damage - oxide charge 21

4.3.2 Detector polarisation 22

4.4 Nuclear reactions 22

5 EXPERIMENTS AND RESULTS **25**

5.1 Irradiation facility 25

5.1.1 5-MV tandem accelerator 25

5.1.2 Cryogenically cooled sample holders 25

5.2 *IV* and *CV* measurements 27

5.3 Determination of Si type inversion 29

5.4 Summary of papers 30

6 CONCLUSIONS **32**

ACKNOWLEDGMENTS **33**

REFERENCES **34**

1 INTRODUCTION

In particle detection, the most common semiconductor detector material is clearly silicon. The advantages for using this second most abundant element in the earth's crust are obvious. Not only are availability and affordability important, but the mechanical properties of silicon are also favourable, and advanced processing methods for silicon-based devices have been developed in recent decades [1]. In addition, the ionisation energy of silicon is small enough to permit easy ionisation, yet large enough to maintain a low dark current, thus making silicon an ideal material for particle detectors.

Silicon particle detectors are widely used in several applications (e.g., space, aviation, and radiation detection). The operation of such devices, however, is compromised when they are irradiated with high fluences (above 5×10^{14} particles/cm^2) of 1-MeV neutrons [2]. In the upgrade of the Large Hadron Collider (Super-LHC, S-LHC) at the European Organization for Nuclear Research (also known as CERN), the silicon detectors will receive a fluence of 10^{16} particles/cm^2 at a distance of a few centimetres from the beam interaction point [3]. This is well beyond the operational limit of current silicon detectors [4]. Thus, more irradiation tests are needed to develop radiation hard detectors.

In addition to the neutron and the electron, a popular irradiation particle is the proton. Proton is a good option for particle irradiation tests, as its defect production rates are several orders of magnitude higher than those of neutrons and electrons, thus allowing shorter irradiation periods with similar beam fluxes. Moreover, in the inner volume of the silicon trackers at LHC, the most damaging particles will be pions. Naturally, such pion irradiation facilities are rare and high fluence pion irradiations are almost impossible to perform, thus it is absolutely necessary to perform proton irradiations as these are the most similar particles to pions when it comes to damage creation in silicon.

Radiation causes in the detector irreversible crystallographic defects, which can be electrically active [5], thus leading to a change in the space charge, leakage currents and trappings. In addition, when traversed by particles, the oxide layers on the surface of the silicon particle detectors become charged. Due to these effects, the risk of a breakdown builds up with the increase in voltage needed to fully deplete the active volume of the detector. Furthermore, the noise of the charge signals rises, and the charge collection efficiency decreases. These detriments can be partly minimised by carefully designing the structure of the detector (e.g., oxygen-rich silicon [6, 7], guard rings) and by cooling the detector.

This thesis explores the development of an irradiation facility with a detector cryocooling system that employs a 5-MV tandem accelerator. The facility allows for the on-line electrical characteristics (current-voltage *IV* and capacitance-voltage *CV*) of the silicon particle detectors. The aim of this thesis was to find conceptual limits for the irradiation of silicon particle detectors with 2 - 9 MeV protons: the decay of proton-induced radionuclides affects electrical characteristics, ionisation caused by the irradiating proton may lead to possible breakdown of the detector, and furthermore, the type of the defect depends on the bombarding energy. A complete experimental assessment of radiation hardness of detectors under operational conditions in future S-LHC experiments is difficult to achieve, making MeV-proton irradiations, such as those used in this thesis, vital in providing fundamental understanding of radiation hardness of silicon particle detectors. Part of the presented work has been carried out in the framework of the CERN RD50 and RD39 collaborations.

2 PURPOSE AND STRUCTURE OF THE STUDY

The main purpose of this thesis was to design, construct and test the irradiation facility for silicon particle detectors. Secondly, the aim of this thesis is to establish conceptual limits for the irradiation of silicon particle detectors with MeV-protons.

The thesis consists of this summary and six articles – printed or under review – in international peer-reviewed journals. The contents of the articles have not been repeated in this summary, but essential background information is provided. The articles are listed below, included after the summary, and referred to in the text by their Roman numerals.

Structure of this summary is as follows. In this Section the list of the articles, as well as the author's contribution to these, are presented. The theory related to characterisation of silicon particle detectors appears in Section 3. The effects of irradiation and their contributions to the electrical characterisations are introduced in Section 4. The experimental arrangements and main results of the articles are presented in Section 5. Finally, the conclusions are presented in Section 6.

2.1 List of articles

The articles listed below are included in the thesis.

Article **I : S. Väyrynen**, P. Pusa, P. Sane, P. Tikkanen, J. Räisänen, K. Kuitunen, F. Tuomisto, J. Härkönen, I. Kassamakov, E. Tuominen, and E. Tuovinen, *Setup for irradiation and characterization of materials and Si particle detectors at cryogenic temperatures*, Nuclear Instruments and Methods in Physics Research A **572**, 978 (2007).

Article **II :** V. Eremin, J. Härkönen, P. Luukka, Z. Li, E. Verbitskaya, **S. Väyrynen**, and I. Kassamakov, *The operation and performance of Current Injected Detector (CID)*, Nuclear Instruments and Methods in Physics Research A **581**, 356 (2007).

Article **III : S. Väyrynen**, J. Räisänen, P. Tikkanen, I. Kassamakov, and E. Tuominen, *Effects of activation by proton irradiation on silicon particle detector electric characteristics*, Journal of Applied Physics **106**, 024908 (2009).

Article **IV : S. Väyrynen**, J. Räisänen, I. Kassamakov, and E. Tuominen, *Breakdown of silicon particle detectors under proton irradiation*, Journal of Applied Physics **106**, 104914 (2009).

Article **V : S. Väyrynen**, J. Härkönen, E. Tuominen, I. Kassamakov, E. Tuovinen, and J. Räisänen, *The effect of an electrical field on the radiation tolerance of Float Zone and Magnetic Czochralski silicon particle detectors*, submitted to Nuclear Instruments and Methods in Physics Research A.

Article **VI : S. Väyrynen** and J. Räisänen, *Effect of proton energy on damage generation in irradiated silicon*, in press, Journal of Applied Physics.

In addition, within RD39 collaboration, the author has contributed to other articles [8–11] related to the topic of this thesis.

2.2 Author's contribution

The author of this thesis is the corresponding author of each article except Article **II**, in which he is a contributing co-author. In each article, the author has performed nearly all of the proton irradiations as well as *CV* and *IV* measurements. The author has played a key role in the development, installation, and testing of the irradiation facility described in Article **I**. The author has coded all computer software relating to the *CV* and *IV* measurements as well to temperature control. The author has carried out all simulations and calculations in Articles **III**, **IV**, and **VI**. He has also played an active role in interpreting the results and in writing the articles. Measurement results presented in this summary, not provided in Articles **I** - **VI**, have been carried out by the author.

3 SILICON PARTICLE DETECTOR

This section introduces the operation principle of the detector and the theory for the characterisation methods used in this thesis and describes the processing of the silicon particle detector. The theory presented here is based on references [5, 12, 13].

3.1 Operation principle of the detector

The detection of energetic particle is based on the collection of generated charge carriers [13]. Ionising radiation (e.g., particles [**III**,**IV**], γ-rays, photons) generates *electron-hole* pairs (EHPs) inside the detector. The average energy required to create *electron-hole* pair (EHP) is 3.62 eV (at 300 K) in silicon, whereas the bandgap is 1.12 eV. The remaining of the energy goes to phonons and plasmons. A depleted diode-junction, introduced in the next section, is used to improve the collection of these charge carriers; the electric field drives the electrons to an anode, and the holes to a cathode. The operation principle of silicon particle detectors is described in Fig. 1. Normally, the electric field is high enough that the drift velocities of the charge carriers become saturated (about 10^7 cm/s). This means that the charge collection time for the charge carriers of a typical detector (thickness 300 μm) is less than 10 ns.

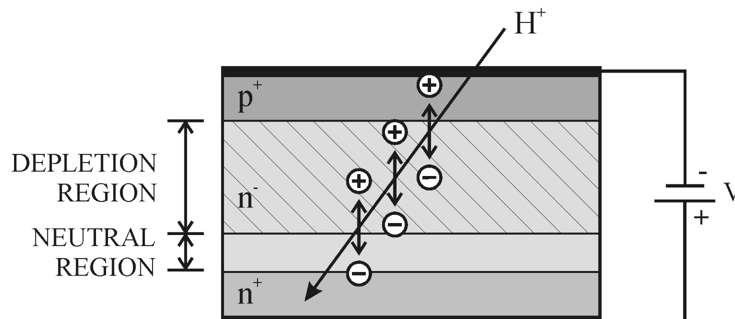

Figure 1: Operation principle of the silicon particle detectors. The particle generates *electron-hole* pairs, which are collected at the electrodes by the electric field in the depletion region.

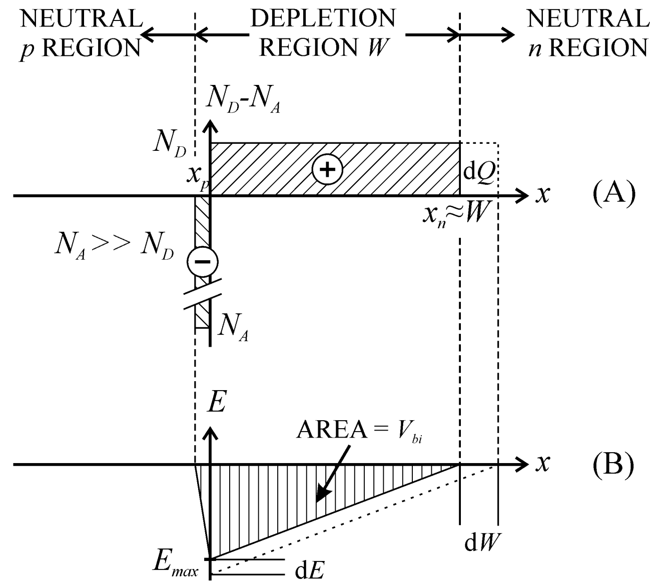

Figure 2: (A) Space charge distribution in a one-sided abrupt junction (p^+n) at thermal equilibrium. (B) Corresponding electric field distribution.

3.2 Diode-junction

While *p*-type material contains a high concentration of holes with few electrons, the opposite is true for *n*-type material. When physically separated *p*-type and *n*-type silicon chips are joined, the diode-junction (a.k.a. *pn* junction) is formed. In device fabrication, the *pn* junction can be formed using a process such as epitaxy, diffusion, and ion implantation (presented in Fig. 5).
The *p*-type region has a net concentration of acceptors N_A (*holes*), and the *n*-type region has a net concentration of donors N_D (*electrons*). Due to the concentration gradient in the *pn* junction, the holes diffuse into the *n*-side, and the electrons diffuse into the *p*-side. Consequently, a negative space charge accumulates on the *p*-side and a positive space charge on the *n*-side. The space charge distribution of an abrupt *pn* junction is illustrated in Fig. 2(A).
For the abrupt junction, Poisson's equations hold:

$$\frac{\mathrm{d}^2\psi}{\mathrm{d}x^2} = +\frac{qN_A}{\varepsilon_S} \quad \text{for} \quad -x_p \leq x < 0 \qquad \text{and} \tag{1}$$

$$\frac{\mathrm{d}^2\psi}{\mathrm{d}x^2} = -\frac{qN_D}{\varepsilon_S} \quad \text{for} \quad 0 < x \leq x_n \quad , \tag{2}$$

where q is the elementary charge, and ε_S is the permittivity of silicon. The overall charge neutrality requires space charges to be equal: $N_A x_p = N_D x_n$.
A typical silicon particle detector has the structure of a one-sided abrupt junction (p^+n or n^+p). This thesis discusses only the p^+n junction, but applicability for the latter is obvious. The depletion layer

width is simply (cf. Fig. 2)

$$W = x_p + x_n \simeq x_n \quad . \tag{3}$$

The electric field in the depletion region [Fig. 2(B)] is given by

$$E(x) = -E_{max} + \frac{qN_D x}{\varepsilon_S} = \frac{qN_D(x-W)}{\varepsilon_S} \qquad \text{for} \quad 0 < x \leq x_n \quad , \tag{4}$$

where E_{max} is the maximum field that exists at junction. Note, at boundaries $x = x_p$ and $x = x_n$, the electric field decreases to zero.
The built-in potential V_{bi} over the junction is given by integrating Eq. (4) over the depletion region:

$$V_{bi} = -\int_0^W E(x)\mathrm{d}x = \frac{qN_d W^2}{2\varepsilon_S} = \frac{1}{2}E_{max}W. \tag{5}$$

Thus, the expression for depletion layer width W is

$$W = \left(\frac{2\varepsilon_S V_{bi}}{qN_d}\right)^{1/2} . \tag{6}$$

The previous equation is valid at thermal equilibrium without external bias. If we apply positive voltage to the n-side, the p^+n junction becomes reverse-biased, and the electrostatic potential across the junction increases by applied voltage V; in Eq. (6), the built-in voltage is replaced by $V + V_{bi}$ or simply by V, because in general, the applied voltage is clearly higher than the built-in voltage (< 1 V) in detector applications. Consequently, the reverse voltage increases the depletion width W.

3.2.1 Capacitance-voltage (CV) characteristics

The depletion capacitance per unit area is defined as $C_j = \mathrm{d}Q/\mathrm{d}V$, where d$Q$ is a change in the charge of the depletion layer per unit area for a change in applied voltage dV. Charge dQ increases the electric field by amount $\mathrm{d}E = \mathrm{d}Q/\varepsilon_S$, and the corresponding change in the applied voltage is approximately $W\mathrm{d}E$ (see Fig. 2). Thus,

$$C_j \equiv \frac{\mathrm{d}Q}{\mathrm{d}V} = \frac{\varepsilon_S}{W} \qquad \mathrm{F/cm^2} \quad , \tag{7}$$

which is the same as the standard expression for a parallel-plate capacitor, where the spacing between the plates is equal to depletion layer width W.
By substituting W from Eq. (6), the junction capacitance is

$$C_j = \left(\frac{q\varepsilon_S N_d}{2V}\right)^{1/2} \quad \Leftrightarrow \quad \frac{1}{C_j^2} = \frac{2V}{q\varepsilon_S N_d} \quad . \tag{8}$$

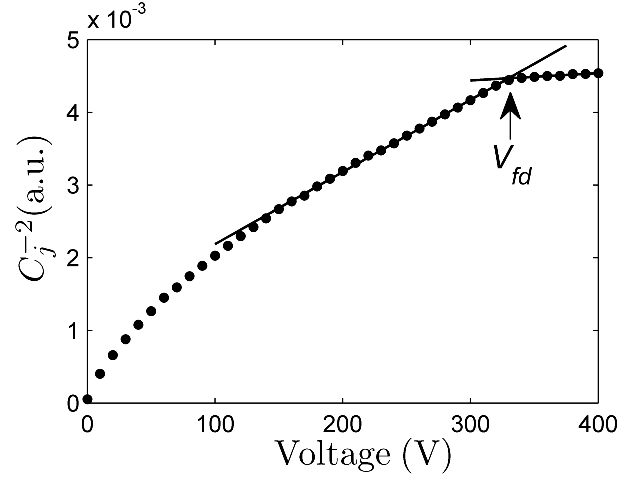

Figure 3: Principle of the determination for full depletion voltage.

This equation is valid when W is thinner than thickness d of the n-side. After full depletion (i.e., the positive space charge is extended to the whole n-side), the capacitance saturates. By plotting CV data on capacitance-voltage characteristics to the (V, C_j^{-2}) graph, full depletion voltage V_{fd}, which corresponds to the capacitance of $C_{fd} = \varepsilon_S/d$, may easily be determined finding the intersection of fitted lines, as shown in Fig. 3, and with this, the doping concentration of the n-side may be calculated by

$$N_d = \frac{2\varepsilon_S}{qd^2} V_{fd} \qquad . \tag{9}$$

The CV-characteristics can also be used to determine heterogeneous doping concentrations [**VI**]. By using Eq. (6), where applied bias V replaces V_{bi} and by deriving Eq. (8), we have

$$\frac{\mathrm{d}C_j^{-2}}{\mathrm{d}V} = \frac{\mathrm{d}C^{-2}/\mathrm{d}W}{\mathrm{d}V/\mathrm{d}W} = \frac{2}{qN_d\varepsilon_S} \qquad ,$$

which yields the equation for determining the doping concentration at depth W:

$$N_D = \frac{2}{q\varepsilon_S \frac{\mathrm{d}(1/C_j^2)}{\mathrm{d}V}} \qquad . \tag{10}$$

Depth W may be determined by using Eq. (7). Another form for Eq. (10) is expressed in reference [14].

Capacitance is typically measured at room temperature and at a frequency of 10 kHz [15], but, for irradiated silicon, capacitance depends on temperature as well as frequency. These dependencies are discussed in Section 4.2.1.

3.2.2 Current-voltage (IV) characteristics

In detector purposes, only biasing with reverse voltage is sensible, leading to increased active volume. The reverse current density (J_R) of a pn junction is the sum of four components: the diffusion current (J_{diff}), the current generated at the surface (J_{sg}), the current generated in the depleted layer (J_g), and the secondary ionisation current at high reverse voltages (J_{si}). For silicon, J_g dominates (despite high voltages), thus the reverse current density is

$$J_R \simeq J_g = \int_0^W qG\mathrm{d}x \simeq qGW = \frac{qn_iW}{\tau_g} \qquad , \tag{11}$$

where G is the rate of *electron-hole* pair generation, τ_g is the generation lifetime, and n_i is the intrinsic charge carrier concentration in silicon. Only energy levels near the intrinsic Fermi level can contribute significantly to generation rate G.
Both n_i and τ_g depend greatly on temperature. Thus, the ratios of current densities J_1 and J_2 measured at different temperatures T_1 and T_2 is given by [16]

$$\frac{J_1(T_1)}{J_2(T_2)} = \left(\frac{T_2}{T_1}\right)^2 \exp\left[-\frac{E_g}{2k_B}\frac{(T_1 - T_2)}{T_1 \cdot T_2}\right] \tag{12}$$

with k_B as the Boltzmann constant ($k_B = 8.6 \cdot 10^{-5}$ eV/K), and E_g as the gap energy in silicon ($E_g =$ 1.12 eV).

3.3 Avalanche breakdown

At high reverse voltages the secondary ionisation current dominates. This phenomenon is known as the avalanche multiplication process. The generated electron acquires kinetic energy from the electric field in the depletion layer. If the field is high enough, the energetic electron can break lattice bonds upon collision with an atom, thereby creating an *electron-hole* pair (secondary ionisation). These created charge carriers similarly acquire kinetic energy from the field and create additional pairs. This process can continue, leading to the multiplication of charge carriers [**III**,**IV**].
In part of the depletion region, the electric field may be high enough for the multiplication process. In such a case both electron (moving rightward in Fig. 2) and hole (moving leftward) concentrations increase equally. The change in electron and hole concentrations in a thin region dx may be expressed as

$$\mathrm{d}n = \mathrm{d}p = \alpha_n n(x)\mathrm{d}x + \alpha_p p(x)\mathrm{d}x \qquad , \tag{13}$$

where $\alpha_{n/p}$ is a field-dependent multiplication coefficient. In general, the holes originate from the multiplication process and hole concentration $p(x)$ may be expressed as $p(x) = n(W) - n(x)$ where W is a boundary of a space charge region. Based on Eq. (13) and assuming that $\alpha_n = \alpha_p = \alpha_{eff}$ (effective ionisation coefficient), the electron concentration may be expressed as

$$n(W) = n(0) + \int_0^W \frac{\mathrm{d}n}{\mathrm{d}x} = n(0) + n(W) \int_0^W \alpha_{eff}(x)\mathrm{d}x \quad . \tag{14}$$

Multiplication factor M is defined as the ratio between electrons leaving and electrons entering the depletion region:

$$M = \frac{n(W)}{n(0)} = \frac{1}{1 - \int_0^W \alpha_{eff}(x)\mathrm{d}x} \quad . \tag{15}$$

The avalanche breakdown voltage is defined as the voltage where M approaches infinity. Thus, the breakdown condition is expressed as

$$\int_0^W \alpha_{eff}(x)\mathrm{d}x = 1 \quad . \tag{16}$$

For the effective ionisation coefficient, the following approximation is assumed [17]:

$$\alpha_{eff} = a_\alpha \cdot E^7 \quad , \tag{17}$$

where E is the electric field and a_α is approximately $1.8 \cdot 10^{-11}$ μm ^{6}/V^7 for silicon.
When the applied bias is greater than V_{fd}, the additional voltage $V - V_{fd}$ drops uniformly over the n-layer with thickness d. Using Eqs. (4) and (5), the magnitude of the electric field becomes [18]

$$E(x) = \left| \frac{2V_{fd}}{d} \left(\frac{x}{d} - 1 \right) - \frac{V - V_{fd}}{d} \right| \quad , \tag{18}$$

where V_{fd} may be solved from Eq. (9).
Regarding Fig. 4, the breakdown voltage as a function of the impurity concentration has been calculated using Eqs. (16) - (18). The avalanche breakdown requires a bias voltage higher than 4 kV for silicon particle detectors with a typical thickness of 300 μm. The avalanche process influenced by surface damage is discussed in Section 4.3.1.

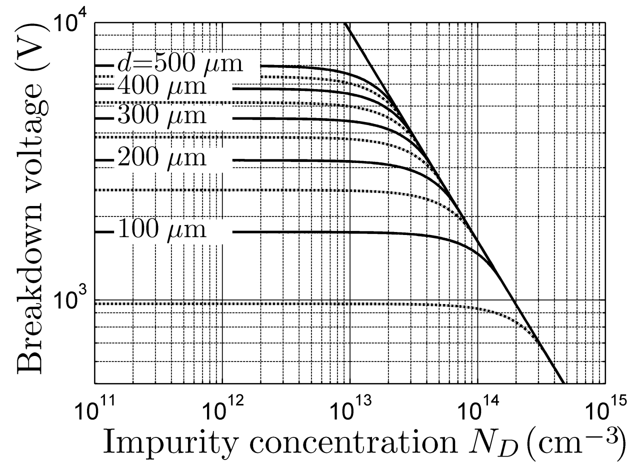

Figure 4: Breakdown voltages calculated for $p^+/n/n^+$-diodes. The concentration of donors N_D and the thickness of d is for the n-layer.

3.4 Processing of silicon particle detectors

Silicon detectors have usually been processed using Float Zone silicon (Fz-Si). Fz-Si has relatively high resistivity (> kΩ), so full depletion of the detector can be achieved at reasonable operating voltages (< kV). Float Zone silicon has a low oxygen concentration (typically < 10^{15} cm^{-3}), however, it has been proved that oxygen improves the radiation hardness of the silicon devices [6]. Silicon wafers made using Czochralski (Cz-Si) method intrinsically contain high concentrations of oxygen (10^{17}-10^{18} cm^{-3}).The resistivity of Cz-wafers is typically not high enough for detector applications. Fortunately, recent developments in the crystal growth technology of Czochralski silicon have enabled the production of Cz wafers with sufficient resistivity and with well-controlled, high concentration of oxygen.

The silicon particle detectors used in this thesis are processed at the Microelectronics Centre of the Helsinki University of Technology using Fz-Si (Topsil, Wacker) and Cz-Si (Okmetic Ltd) wafers as starting materials. The structure of the detectors was processed essentially in the following manner: the p^+-layer (boron) was implanted on the front surface (anode) of the n-type bulk material, and the n^+-layer (phosphorus) on the backside (cathode). The backside implantation enables overdepletion of the detector. The aluminium layers ($\sim$ 0.5 μm) are then sintered to the electrodes, thus providing the electrical contacts. Fig. 5 shows the process steps of the silicon particle detector. A more detailed process flow is described in references [19, 20].

In the actual detector concept used in this work, the active area (front electrode, 5 × 5 mm^2) is surrounded by one or several guard rings (p^+-doped) against the effects of cutting edges and to smooth the electric field. In general, the guard rings are grounded. The oxide layer (0.2 to 1 μm thick) covers the non-metallised regions on the detector surfaces. The outer dimensions of the detectors were either

7×7 mm^2 or 8×8 mm^2. A typical thickness for Si-detector is about 300 μm, whereas the thickness is $\sim$ 7 μm for the n^+-layer and $\sim$ 3 μm for the p^+-layer. A cross-sectional view of the detector is shown in Article **IV** (Fig. 1). A photograph of the detectors is shown in Fig. 6.

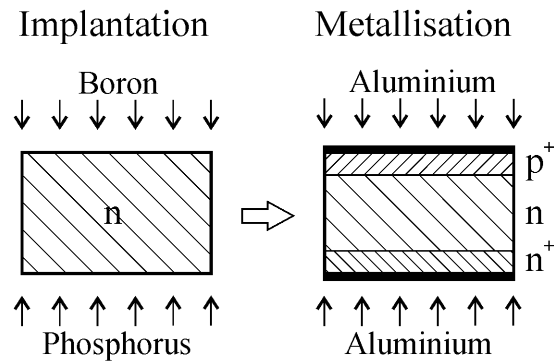

Figure 5: The principle of processing a silicon particle detector. The n-type Si-chip is implanted with boron and phosphorus on the front and backside, respectively. Aluminium electrodes are then sintered to provide electrical contacts.

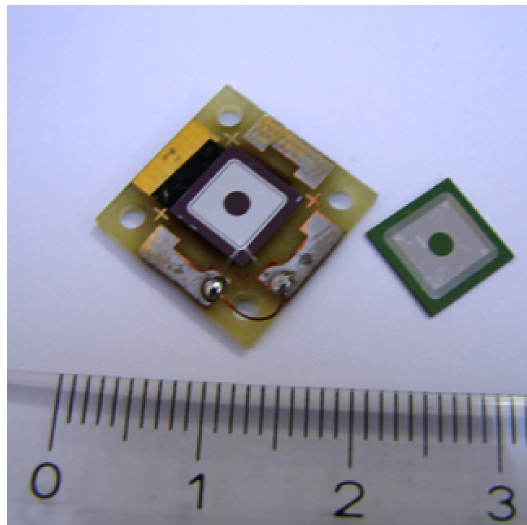

Figure 6: Photograph of the silicon particle detectors. On the left, the detector is attached to a printed circuit board (PCB) pad, which facilitates the characterisation measurements.

4 IRRADIATION EFFECTS

This section discusses the interactions of detector materials, especially of silicon, with MeV-range protons. Contributions of the irradiation effects to the detector operation are also introduced.

4.1 Interaction processes

When an energetic proton hits silicon, various types of interactions may occur, as is shown in Fig. 7. For example, protons can scatter from the Si-atoms (elastic and inelastic scattering), which can then recoil, or they can ionise the atom by kicking off the inner shell electrons, leading to the characteristic emission of X-rays or Auger electrons. In addition, some proton-induced nuclear reactions can lead to the emission of γ-rays. In this context, however, we are interested mainly in phenomena essential to the operation of the detector, namely displacement damage resulting from proton bombardment, the energy loss of protons in silicon, and radionuclide production [**III**].

Energy loss is an important term in ion beam physics and is often referred to as stopping power [21]. Stopping power means the average energy loss of the particle per unit path length ($S \equiv \mathrm{d}E/\mathrm{d}x$). Depending on energies used, the stopping power is divided into two groups: nuclear and electronic stopping. Only the former may cause displacement damage (i.e., the non-ionising energy loss), but both classes contribute to the ionising process. Electronic stopping is orders of magnitude stronger than nuclear stopping at MeV energies (Fig. 8), thus in practical terms, the ionising energy loss corresponds to the total energy loss. One useful term relating to energy loss is projected range R_p, defined as the mean depth from the target surface at which the ion stops. The R_p takes account of the

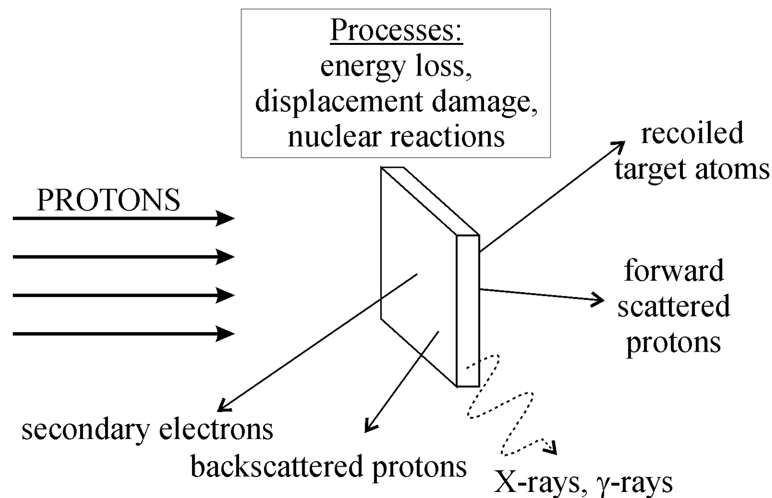

Figure 7: Interactions that occur when protons hit the matter.

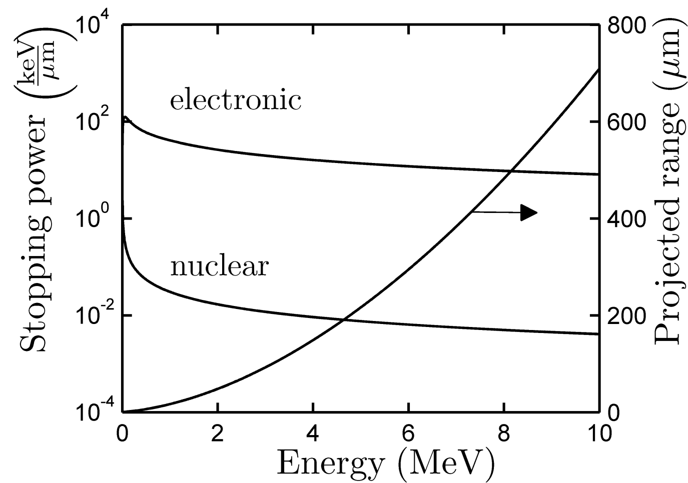

Figure 8: Electronic and nuclear stopping powers and projected ranges for protons in silicon.

real path of particles (i.e., of the lateral straggling) also. Fig. 8 shows the dependence of the stopping powers and the projected range of protons in silicon on the bombarding energy. The stopping powers and the projected ranges used in this thesis are calculated by SRIM-code [22].

4.2 Bulk damage - non-ionising energy loss

A low concentration of defects in silicon are already present before irradiation, and energetic particles cause additional defects in the material bombarded. These defects are roughly categorised as clusters and point defects. Low-energy electrons cause point defects, whereas neutrons cause mainly the clusters. Protons create both of them, but the point defects predominate at several MeV energies. This phenomenon is tested in Article **I** with positron annihilation spectroscopy by irradiating Si-sample with 9.5-MeV protons.

The simplest defect in silicon is an interstitial-monovacancy pair, known as a Frenkel pair, in which the Si-atom is displaced from its lattice site to the interstitial. An important parameter for describing radiation damage is the threshold energy for displacement. For silicon, this is 36 eV, on average [23], which indicates a minimum energy of 1 keV for protons colliding with a Si-atom at rest. However, the probability of colliding with a small impact parameter, defined as a perpendicular distance from the projectile's path to an atom at rest, is very small [24]. Thus, the energy needed for protons to displace a Si-atom is clearly higher on average. The Si-atom can acquire enough kinetic energy in such a collision to form an extra Frenkel pair, and the initial displacement gives rise to a series of cascades which stop when the kinetic energy of the dislodged atom is less than the threshold [25].

The monovacancies are already mobile at moderately low temperatures (> 100 K [26]) and can move

some distance through the Si-lattice. They can disappear from the material by recombining with the interstitial atom or by moving to the surface. Interstitials can behave similarly, but of course, recombination occurs with the vacancy. If one of the components of the Frenkel pair is lost to the surface, the remaining component is known as a Schottky defect.
Alternatively, monovacancies can combine to form a more complex and larger vacancy, which constitutes a moderately stable defect. In the case of interstitials, they can accumulate in the Si-bulk to form stacking faults. The mean free path between two successive collisions decreases towards the end-of-range, where the interaction of defects strengthens. More commonly, mobile vacancies and interstitials become trapped by impurity atoms, which gives rise to stable defects or defect complexes. The most common impurities in Si include oxygen and carbon, and the doping impurities of phosphorus and boron which are used to modify the sign of charge carriers (n or p). Vacancies appear to have an affinity for atoms which release electrons, such as P, As, and Sb (donor dopants), and less for elements with a deficiency of electrons (acceptor dopants).

4.2.1 Effects of defects on detector properties

Many defects are electrically active and can be classified according to their electrical properties as acceptors or donors. Some of the defects have more than one energy level in the band gap. These are known as amphoteric defects with an acceptor and donor level in the band gap.
Radiation-generated defects have complicated electrical properties [5, 27]. The defects will have the following main consequences. (A) *They can change the charge density of the space charge region* [**V**,**VI**]. Usually levels in the lower half of the band gap are occupied by electrons in the depletion region, while those in the upper half are not. This means that, if a donor exists below the mid-band gap or if an acceptor exists above that, they are neutral in the space charge region. Conversely, when an acceptor exists in the lower half of the band gap or if a donor is in the upper half, they are ionised and contribute negative and positive space charges. Thus, the defects generated by irradiation affect the full depletion voltage of the detectors (Eq. 9). (B) *They act as recombination-generation centres* [**I**,**V**,**VI**]. The presence of a donor or acceptor near the conduction or valence band is known as a shallow level. On the other hand, the levels near the mid-band gap, the deep levels, can serve as generation and recombination centres, and if they are located in the depletion layer, they increase the leakage current of the detector (Eq. 11). (C) *They act as trapping centres* [**II**,**IV**]. Electrons or holes are captured and re-emitted with a time delay.
Several radiation-damaged mechanisms lead to a change in the space charge, which is categorised as the removal of donors (e.g., vacancy-phosphorus complexes), the removal of acceptors (e.g., vacancy-boron complexes), the creation of defects assuming positive charge states in the space charge region (effective "donors"), and the creation of defects assuming negative charge states in the space charge

region (effective "acceptors"). These are expected to depend on irradiation fluence Φ, and the effective doping concentration is parameterised as [5]

$$N_{eff}(\Phi) = N_{D,0}e^{-C_D\Phi} - N_{A,0}e^{-C_A\Phi} + b_D\Phi - b_A\Phi \tag{19}$$

where $N_{D,0}$ and $N_{A,0}$ are the initial concentrations of donors and acceptors, and c_D, c_A, b_D and b_A are constants determined experimentally. N_{eff} can be determined from CV-data by Eq. (9), but a simple measurement of the detector depletion voltage provides information only on the difference between effective donors and acceptors. Many papers [28–31] state that the depletion voltage of the $p^+/n/n^+$-detector decreases with irradiation fluence until it begins to increase: the space charge region changes the sign from n to p [32]. The type inversion leads to a $p^+/p/n^+$-structure in which the detector, unlike non-irradiated detector, begins to deplete the pn^+-junction. For heavily irradiated detectors, the so-called double peak effect emerges: the depletion layer begins to deplete from both sides [31]. As may be noted, the CV characteristics depend on the temperature and frequency used for irradiated detectors. In the CV measurement, an AC test signal is superimposed on the constant applied bias. Due to this AC signal, those deep traps near the edge of the depletion region switch between the depleted and the neutral regions. In the depleted region, they are empty and, thus, contribute to the space charge of the device, whereas in the neutral region, they are filled being neutral. If the frequency of the charging current of the capacitance device is sufficiently low, the process of filling and re-emptying the traps will be measured. Conversely, at sufficiently high test signal frequencies, the measurement will be insensitive to the presence of the deep traps, so the material seems to be essentially intrinsic. The maximum frequency for a deep-level charging is proportional to temperature T as follow [33]:

$$f \propto T^2 \exp\left(-\frac{E_a}{k_B T}\right) \quad , \tag{20}$$

where E_a is an energy level between the energy level of the deep trap and of the conduction or valence band. In conclusion, at lower temperature, the lower frequency for the charging signal of the CV device is needed. The capacitance-voltage measurement will flatten for irradiated detectors at lower temperatures, when a constant frequency is used, as is shown in Fig. 9.

Similarly, the defects with deep levels, which cause the bulk current, are expected to depend on the fluence. If normalised to sensitive volume V, change of current ΔI has proved to be proportional to 1 MeV neutron equivalent fluence $\Phi_{eq.}$, and the following expression holds [34]:

$$\frac{\Delta I}{V} = \frac{\Delta J_R}{d} = \alpha\Phi_{eq.} \quad , \tag{21}$$

where α is a current-related damage rate. If α is determined after an annealing of 80 min at 60 °C and normalised to 20 °C, α is a universal constant independent of the detailed history of the

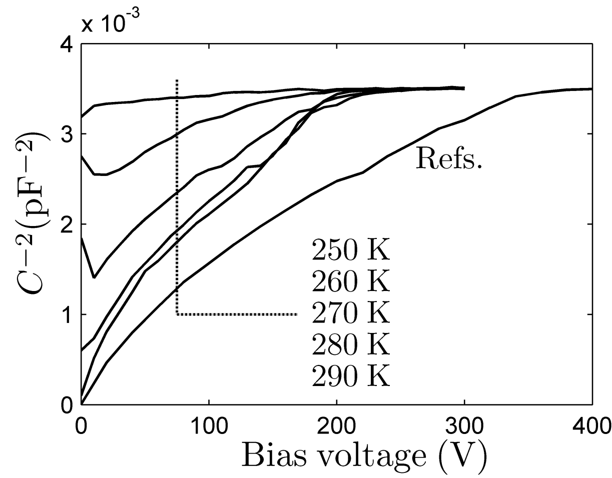

Figure 9: The *CV* curves of an irradiated Czochralski detector measured at different temperatures (the curve at top represents the lowest temperature). Reference curves measured at 290 K and 250 K prior to irradiation overlap and are shown for comparison. The frequency used was 18 kHz.

actual irradiation and of the type of material (n or p, Float-zone or Czochralski, resistivity, etc.), or irradiating particles (protons, neutrons, pions).

4.2.2 NIEL scaling hypothesis

Several experimental observations have led to the assumption that damage produced in the silicon bulk caused by particle bombardment can be considered proportional to so-called displacement damage cross-section D, which is equivalent to non-ionising energy loss (NIEL). The proportionality between the NIEL value and the damage caused by particles is referred to as the NIEL scaling hypothesis, and the NIEL values are used to normalise the different irradiation effects of various particles over large energy regions. According to ASTM (the international standards organisation) standards, the displacement damage cross-section for 1 MeV neutrons is set to a normalising value.
Proton irradiation fluence Φ is converted to the 1 MeV neutron equivalent with the following equation:

$$\Phi_{eq} = \kappa\Phi = \left(\frac{1}{d}\int_{x_0}^{x_d} \kappa(E_x)\mathrm{d}x\right)\Phi \qquad , \tag{22}$$

where κ is an energy-dependent hardness factor. Fig. 10 presents the hardness factor as a function of proton energy. Because of the finite dimensions of detectors, the hardness factor must be determined taking into account of the energy loss: in brackets in Eq. (22), d is the thickness of the active layer, x_0 is the width of the dead layer, and $x_d = x_0 + d$. The energy values at depth x may be determined from Fig. 8.

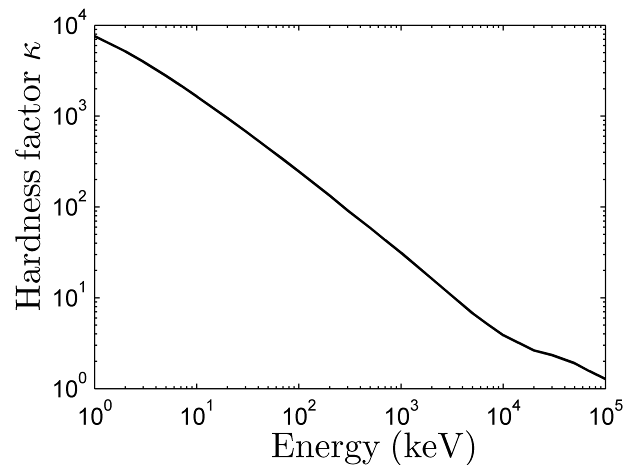

Figure 10: Hardness factor for an energetic proton as a function of proton energy. Data are from ref. [37].

NIEL scaling is regularly used in comparisons between damages produced in experiments with different particles and energies. However, studies have not established microscopic understanding of why damage should scale with NIEL, and some experiments [35, 36] even argue against it. Violations of NIEL scaling preclude its use as strict rule, but it is nevertheless a useful tool for comparing most particles and energy dependencies of the damage observed in silicon particle detectors.

4.3 Ionising energy loss

4.3.1 Surface damage - oxide charge

The surface oxide already contains a large number of defects even before incurring damaging irradiation. The highest concentration of damage is in the silicon-oxide interface.
Ionising radiation also creates $electron - hole$ pairs in the oxide. In the silicon lattice, EHP creation is a completely reversible process with no damaging effects. But this is not true of surface oxide [38]: depending on the electric field, a part of the EHPs fails to recombine. The mobility of *electrons* are rather high in the oxide and have a high chance of diffusing from the oxide, whereas for *holes*, the mobility is low, leading to a positive charge buildup in the oxide [39]. In addition, the electric field directed away sweeps the *holes* created elsewhere towards the oxide [38], thereby increasing the oxide charge. Basically, the saturation of positive oxide charge buildup is achieved when all *hole*-trapping defects are filled. Another explanation for this is that a positive trapped charge creates an electric field which prevents the escape of electrons [40]. The irradiation creates more trapping defects to the oxide, and the saturation value of the oxide charge is dependent on the irradiation fluence [38, 40]. The saturation value achieves its maximum at a fluence of about $3 \cdot 10^{13}$ p/cm^2 for 7 MeV protons.

In the present detector structure, metallisation is slightly extended over the oxide [Article **III**, Fig. 1] forming a metal-oxide-semicondutor (MOS) capacitor structure, in which the oxide has the positive charge. The oxide charge saturates to a value of the order of $2{\cdot}10^{-7}$ C/cm^2 [38, 39]. Assuming a thickness of 500 nm and a relative permittivity of 4 for surface oxide, the voltage change over the oxide is $\Delta V_{ox} = \Delta Q_{ox}/C \approx 30$V. This leads to a strong electric field near metal-semiconductor and metal-oxide-semiconductor interfaces, and thus the avalanche breakdown process would occur [**III**,**IV**].

4.3.2 Detector polarisation

The main component of reverse current is the bulk generation current, which decreases exponentially with temperature [Eqs. (11) and (12)]. Therefore, to minimise the reverse current, the detectors are cooled during the experiments. When EHPs are generated in the detector by light illumination or ionising particles, some charge carriers may be trapped. Unfortunately, the trapping of charge carriers in deep levels increases at lower temperatures. The trapping causes changes in the electric field, a phenomenon referred to as detector polarisation. Thus, when constant bias is applied, detector polarisation can change the mode of the detector from full-depletion to partial-depletion [**IV**].
The concentration of trapped carriers increases with time [41], and the effective space charge density changes by $N_{eff}(t) = N_{eff}(0) \pm n_t(t)$, where n_t is the concentration of traps with a positive sign for hole trapping and a negative sign for electron trapping, respectively. At a given bias V, full-depletion is achieved with the critical effective concentration $|N^*_{eff}|$, and the depletion width is related to N_{eff} as follows:

$$W = \begin{cases} d & \text{for} \quad |N_{eff}| \leq |N^*_{eff}| \\ \sqrt{\frac{2\varepsilon_S V}{e|N_{eff}|}} & \text{for} \quad |N_{eff}| > |N^*_{eff}|. \end{cases} \tag{23}$$

When $|N_{eff}| > |N^*_{eff}|$, W becomes smaller than full depletion width d, and the detector is changed to the partial-depletion mode.

4.4 Nuclear reactions

Low energy protons scatter elastically from nuclear potential, but when energy increases, so does the probability to penetrate the potential wall, and – depending on the reaction threshold energy – nuclear reactions are possible. Fig. 11 presents on the left the most typical radiation-induced nuclear reactions, and in the middle, the decay channels of radionuclides. In the case of protons, (p,n)- and (p,γ)-reactions are possible, but cross-sections of the (p,n)-reactions are typically three orders of

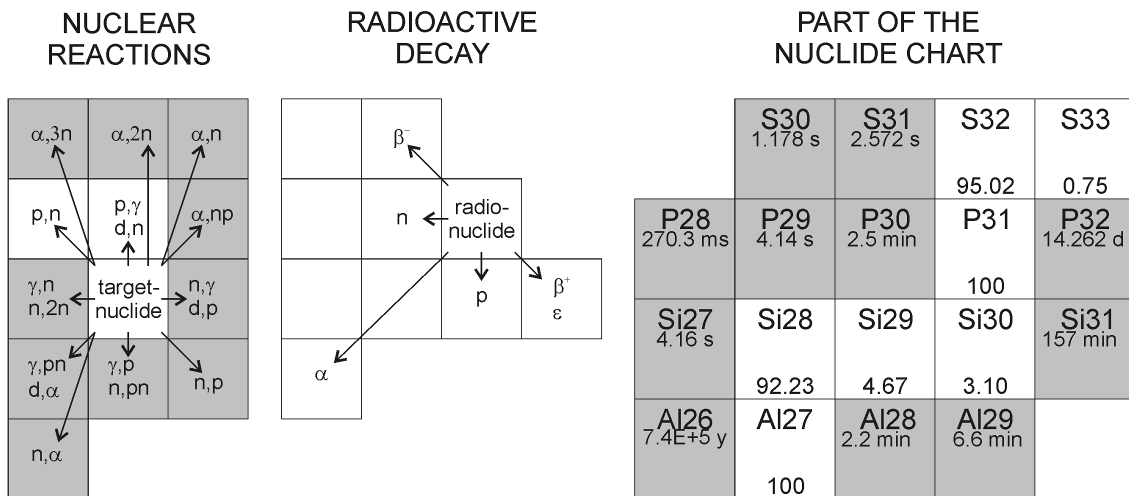

Figure 11: Particle-induced nuclear reactions. Left, nuclear reactions with the proton-induced reactions shown in white. Middle, the decay schemes of the radionuclides. Right, part of the nuclide chart in which the radionuclides are hatched. The graphics are modified from the Karlsruhe nuclide chart [42].

magnitude higher than those of (p,γ)-reactions. The nuclides produced are often radioactive and decay by emitting positrons [**III**] or by the electron capture process.

The nuclear cross-section is one important parameter needed to estimate the quantity of effects: the higher the cross-section, the more daughter nuclides are produced. The number of nuclides A per unit area produced in the sample with thickness d may be calculated as

$$A = \Phi \int_0^d \sigma[E(x)]N(x)\mathrm{d}x \qquad , \tag{24}$$

where σ is the reaction cross-section, and N is number of isotopes per cm^{-3} in the sample irradiated to the fluence Φ.

The other parameters include the threshold energy of the reaction and the half-life of the radionuclide produced. With short half-lives compared to the duration of the irradiation or the measurement, the decay of the radionuclide is affected instantly, whereas with longer half-lives, the effect arises later.

Si is used in detector concepts, of course, but aluminium and gold electrodes, for example are used in electrodes with elements of the detector holder (e.g., steel and electric wires). The concentration of dopant impurities (e.g., B, P, and As) is usually very low, and their contributions to the nuclear reactions are negligible. The reactions with some materials in the detector concept and their threshold energies for protons are tabulated in Table 1. In addition, the half-lives of daughter nuclides are also presented. Fig. 12 shows the corresponding cross-sections.

Table 1: Proton-induced reactions in detector-related materials. Data are taken from Ref. [43].

Reaction	Threshold (keV)	Product half-life
^{27}Al(p,n)^{27}Si	5804	4.2 s
^{29}Si(p,n)^{29}P	5924	4.1 s
^{30}Si(p,n)^{30}P	5183	2.5 min
^{56}Fe(p,n)^{56}Co	5183	77 d
^{63}Cu(p,n)^{63}Zn	4215	38.5 min
^{65}Cu(p,n)^{65}Zn	2168	244 d
^{197}Au(p,n)^{197}Hg	1390	64 h

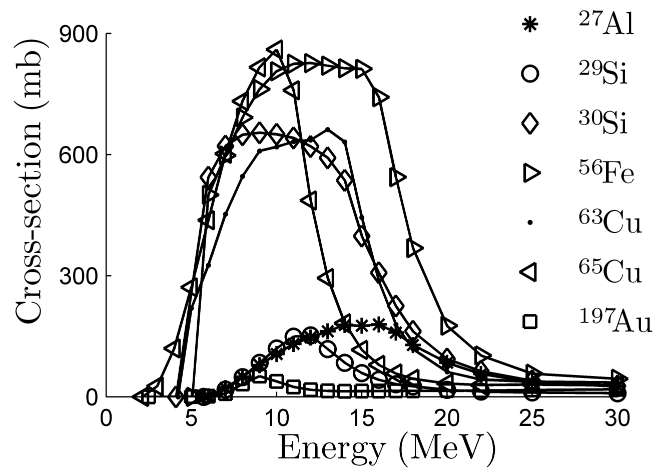

Figure 12: Cross-sections of (p,n)-reactions for target materials used in the detector structure. Data are taken from Ref. [44].

5 EXPERIMENTS AND RESULTS

The facility for the irradiation of Si-detectors with protons is expressed in the beginning of this Section. The characterisation methods are later introduced, and the main results of the Articles included in this thesis are highlighted.

5.1 Irradiation facility

5.1.1 5-MV tandem accelerator

The accelerator is a vertical belt-driven 5-MV tandem of the EGP-10 type and was installed at the University of Helsinki in 1982. Over the years, the accelerator has undergone several upgrades (e.g., the manual controls of all essential parameters are computer-controlled). Therefore, despite its physical dimensions, this accelerator is competitive to more recent ones. More detailed specifications of the accelerator and its latest upgrades can be found in Refs. [45, 46].
The accelerator has three ion sources, of which a miniature ion-sputtering source is used to produce negative hydrogen ions. From the ion source (electrically grounded), extraction voltage V_S (max. 40 kV) steers the ions to the inclined-field accelerating tube via an injection magnet. The acceleration tube and a high-voltage terminal (V_{HV}) is located in a pressure tank, where a gas mixture of CO_2+N_2 (20:80) at a pressure of 12-14 bar provides the electrical insulation. The negative ions entered the accelerating tube gains kinetic energy in a high electric field, and in the terminal, the ions enter the stripper gas (CO_2 or Ar) channel, where their electrons are stripped, thus rendering them positively charged (charge Q). The positive ions accelerate up to the analysing magnet (grounded), where the mass and energy are chosen. Finally, the energy of the ion is $E = q(V_S + V_{HV}) + QV_{HV}$. After the analysing magnet, the ions are steered to the measurement chambers.
For protons, the maximum energy is 10 MeV (routinely 9.5 MeV), while the minimum is about 1.8 MeV. The difference in energy is less than 10 keV. Values for the ion beam currents in the measurement chamber are a maximum of about 400 nA and a minimum of about 0.5 nA, and the fluctuation is about 10%.

5.1.2 Cryogenically cooled sample holders

A novel facility for proton irradiation with sample cryocooling by a helium cryostat was developed in 2006 and employs the 5-MV tandem accelerator [Article **I**]. The facility allows damage generation to the detectors and their on-line studies of electrical characteristics as well as the positron annihilation

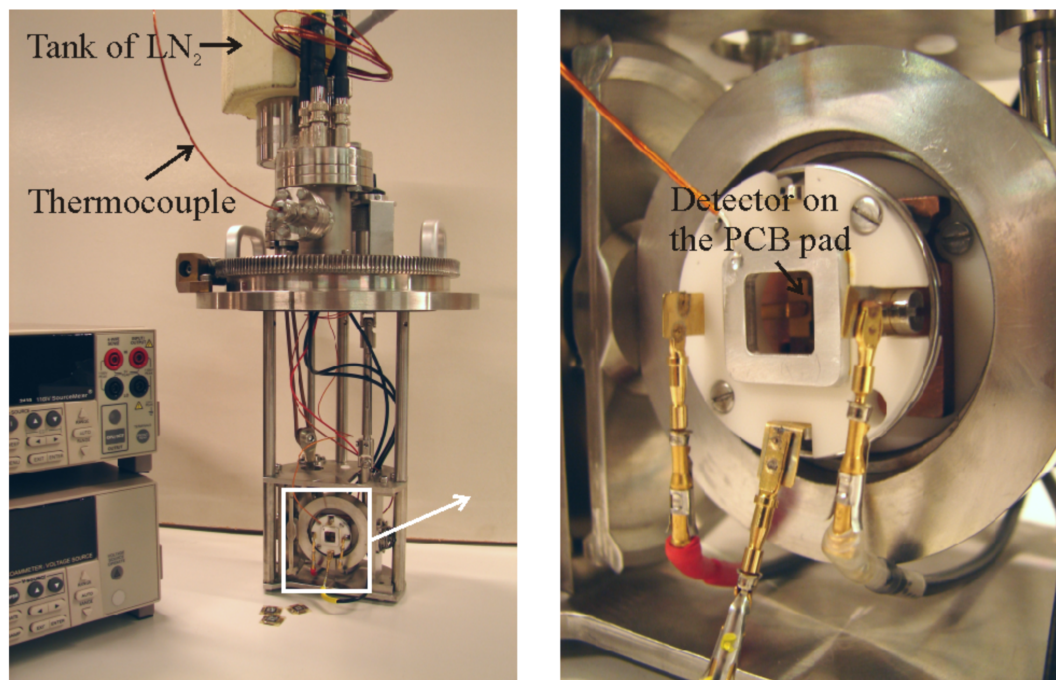

Figure 13: Liguid nitrogen (LN_2) cooled goniometer.

spectroscopy. For detector irradiation, the minimum temperatures achieved are about 50 K and 70 K both with and without a thermal radiation shield, respectively, while the maximum is about 400 K (limited by degradation of the vacuum).

The irradiation temperature is often clearly higher than the minimum limits mentioned, so the liquid nitrogen-cooled sample holder was developed primarily to quicken sample cooling and heating. For this purpose, a sample holder in a four-axis goniometer was equipped with an LN_2-cooling system. In addition, the heating resistor was installed in the holder, so it is possible to keep the temperature of the detector on the PCB-pad (Fig. 6) between 110 K and 400 K. This goniometer also permits so-called channelling studies at different temperatures in other research activities.

Without the insulating pad, the minimum temperature for the sample would be about 90 K. The cooling rate for the detector on the PCB-pad is about 11 K/min, and the maximum rate for heating is about 40 K/min. The corresponding values for the cryostat are 4 K/min and 10 K/min, respectively.

For the goniometer, the new detector holder for characterisation purposes was designed to be easier to use than its predecessor (Article **I**, Fig. 5) and to permit measurement of the the beam current by the collimator [Article **III**, Fig. 1(b)]. The new holder is compatible with the cryostat. Photographs of the goniometer and the sample holder appear in Fig. 13.

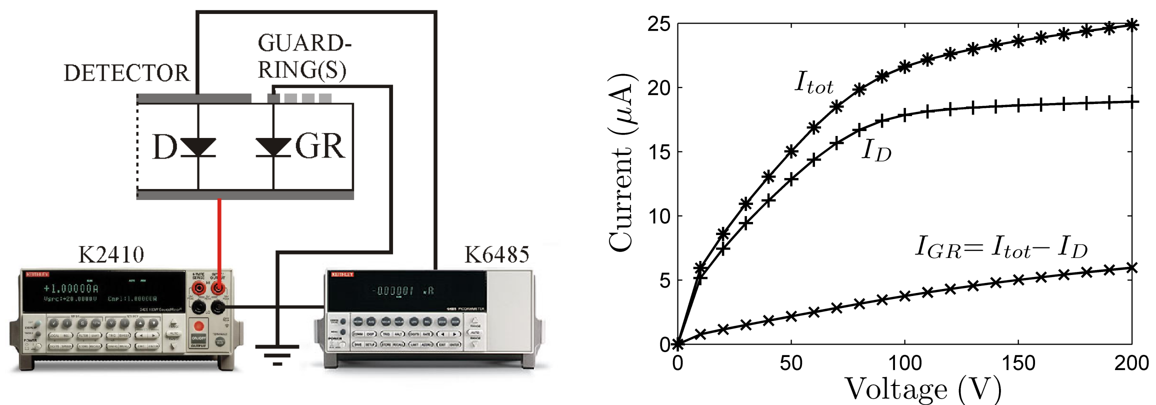

Figure 14: Left, the wiring diagram for measurement of the current-voltage characteristics of silicon particle detectors with a Keithley 2410 SourceMeter and a 6485 Picoammeter. Right, *IV*-curves of a Czochralski-detector irradiated with 7-MeV protons up to a fluence of 10^{13} protons/cm^2.

5.2 *IV* and *CV* measurements

The detector structures have at least one guard ring, which delineates the area of the detector and protects it against edge effects. So, in practice, there are two parallel diodes: the actual detector (D) and the guard ring-diode (GR). Thus, the overall current (I_{tot}) from the voltage source is divided.
In our setup, the active area is grounded via a current meter (current I_d), and the inner-most guard ring is grounded directly ($I_{GR} = I_{tot} - I_D$). An ungrounded guard ring can lead to drastically skewed leakage current values due to the undetermined active volume of the diode [47]. The opposite side of the detector (n^+ side) is positively biased by a source meter, where the current (or voltage) meter and the voltage (or current) source are combined. Keithley models 485, 6485 and 6487 served as the current meters. The last device can also serve as a voltage source (up to 505 V), but usually Keithley 2410 is used with an extended voltage range (1 kV). The current noise in *IV* measurements is less than 0.1 nA. Fig. 14 shows a schematic of electrical couplings as well as examples of the total and detector currents.

Commonly, ammeters are believed to have very low impedance, but when the measuring current decreases, the impedance of the ammeters increases. If the resistance between the front electrode and the inner-most guard ring, which may depend on currents and applied voltage, is relatively small, a careful interpretation is needed. This may be checked easily by also measuring I_{GR} when the detector-electrode is grounded or by using an additional current meter for I_{GR} [48]. The sum of measured currents I_D and I_{GR} should be equal to I_{tot}.
A source meter combined with a capacitance meter enables determination of the *CV* characteristics of the detectors. The capacitance meter used in this work was built at CERN and was developed especially for detectors with high reverse currents. This device uses a charging frequency of 18 kHz and involves voltages of up to 600 V. The capacitance meter can measure capacitance up to 500 pF with a

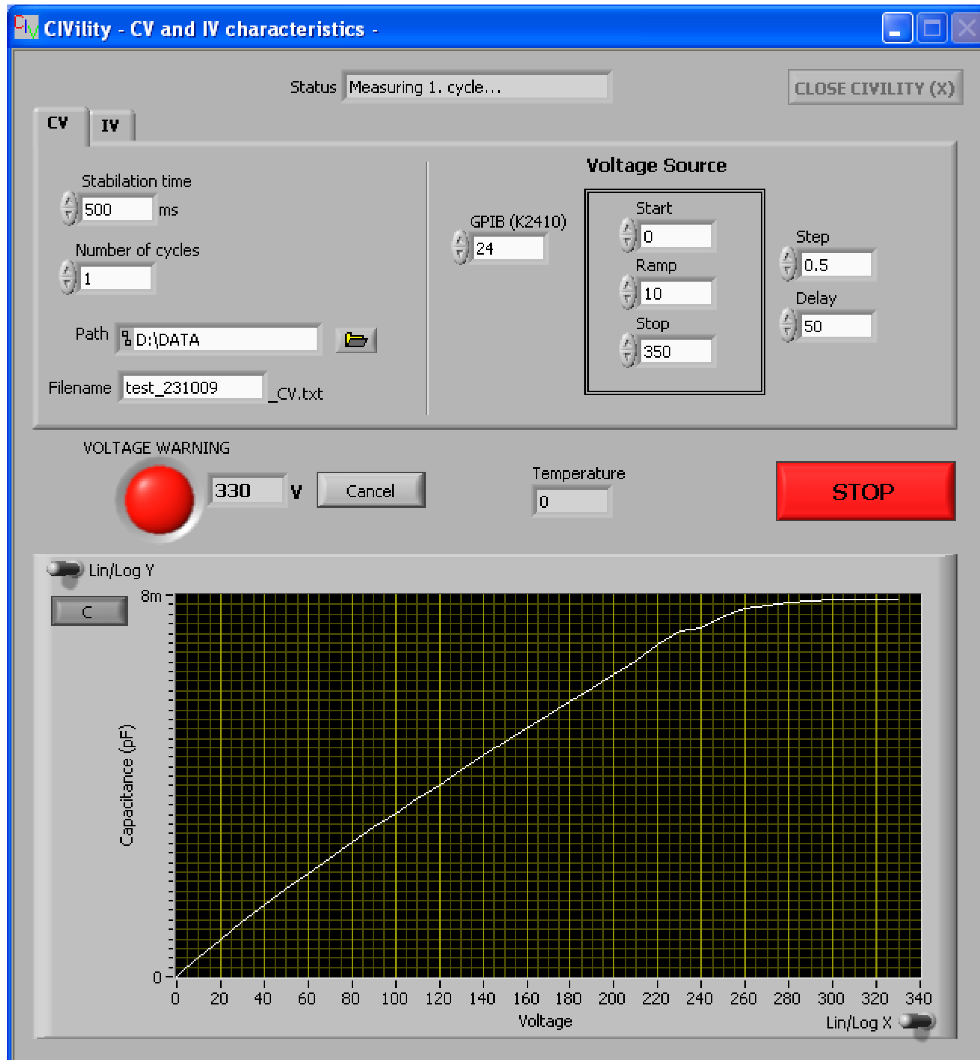

Figure 15: Screenshot of the graphical user interface for *CV* and *IV* measurements.

resolution of less than 0.1 pF. The capacitance meter has been compensated for parallel capacitances (e.g., wires) on which its accuracy mainly depends.

In *CV* measurements, both front electrodes (D and GR) are grounded, and capacitance is measured from the whole detector structure. Capacitance could be measured with the floating GR, but then full depletion occurs at higher voltages.

The current meters and source meters are connected to a computer via GPIB (General Purpose Interface Bus), and the graphical user interface (GUI) for *IV* measurements was previously coded by Matlab [Article **I**]. But when measurements of the *CV* characteristics began, the interface was developed with LABVIEW. The screenshot of the graphical user interface for the *CV* and *IV* measurements appears in Fig. 15.

5.3 Determination of Si type inversion

Type inversion has been estimated to occur by following the evolution of the full-depletion voltage determined by *CV* measurements with irradiation fluence (Fig. 16, left). At the turning point, the space charge sign inversion is believed to arise. But a single V_{fd}-measurement makes no indication of whether the detector type is inverted or not, although it is possible with a few other methods: by using the transient current technique (TCT) [49], optical beam-induced current (OBIC) and surface potential (SP) measurements [50], or a scanning electron microscope [30].

In this work, a new method was developed to exploit the short range of α-particles in silicon. Our α-source is a mixture of α-emitting nuclides (^{233}U,^{238}Pu,^{239}Pu) with the most intense peaks at 4.8 MeV, 5.2 MeV, and 5.5 MeV. An energy of 5.2 MeV for an α-particle corresponds to a range of about 26 μm in silicon [22]. When the $p^+/n/n^+$-structure is used (cf. Fig. 5), the space charge layer begins to increase from the p^+-side. If α-particles enter the detector from this side, the collection of EHPs generated by α-particles achieves the maximum value until the depletion layer width is as wide as the range of the particle. However, if α-particles hit the detector from the opposite side (n^+), the collection of EHPs peaks when the detector is fully depleted. The opposite is true for a $p^+/p/n^+$-structure.

The charge generated in the detector was collected with a low-cost charge-sensitive preamplifier (Cremat CR-110 [51]) with a sensitivity of 1.4 V/pC, equal to 62 mV/MeV for Si-detectors. For an output of the preamplifier that is proportional to the number of EHPs generated, the rise time is about 12 ns for detectors with a capacitance of 12 pF, whereas the decay time is about 140 μs. A basic oscilloscope (e.g., Tektronix TDS series [52]) may serve to determine the pulse height. The evaluation board of Cremat CR-150 with a bias resistor of 10 MΩ, and a Keithley 2410 were used to apply and to measure the bias voltage.

In Fig. 16, left, the full depletion voltages of irradiated Float-zone (Fz) and Czochralski (Cz) detectors are shown. The Cz-detectors have not been type-inverted at fluences below $3.4 \cdot 10^{13}$ p/cm^2, whereas the Fz-detectors seem to be type-inverted already at the lowest fluence of $6 \cdot 10^{12}$ p/cm^2. For testing purposes, a non-irradiated *n*-type detector and a detector irradiated to the fluence of $1.7 \cdot 10^{13}$ p/cm^2 were bombarded by α-particles from both sides and the collected EHPs as a function of bias voltage are shown on the right in Fig. 16. For the non-irradiated detector, the collected EHPs achieve maximum at low voltages, when α-particles hit the detector from the front side (p^+), whereas maximum of the collected EHPs is achieved at higher voltages for the type-inverted detector.

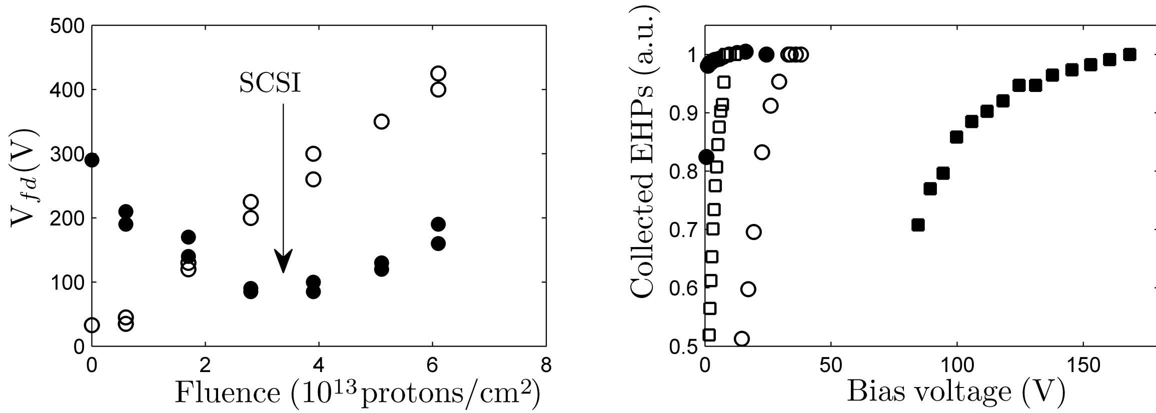

Figure 16: Left, the full depletion voltage as a function of an irradiation fluence of 9 MeV protons. The open symbols indicate the Float-zone detectors, and the filled symbols, the Czochralski detectors. For the Cz-detectors, the space charge sign inversion is seen at a fluence of about $3.4 \cdot 10^{13}$ p/cm^2. Right, the collected EHPs generated by 5.2 MeV α-particles from the Fz-detectors appear as a function of the bias voltage. The circles were measured from the non-irradiated detectors, and the squares from the type-inverted detectors first irradiated with protons up to the fluence of $1.7 \cdot 10^{13}$ p/cm^2. The filled symbols denote α-particles that hit the detector from the p^+ side, and the open symbols, from n^+ side.

5.4 Summary of papers

In Article **I**, the irradiation facility was tested by irradiating magnetic Czochralski (MCz) detectors at 240 K with 9 MeV protons to a fluence of 2.5 $\times 10^{15}$ cm^{-2}. After irradiation, the temperature was reduced to 116 K, and *IV* curves were measured at fixed temperatures between 184 K and 241 K. The reverse current level of the irradiated detector was considered relevant, and its dependence on temperature was observed to correspond to Eq. (12). In addition, a current-injected detector (CID) was also irradiated in Article **II**. In a CID, current injection modifies the electric field distribution in the detector bulk [53]. The injection of a charge took place via a forward-biased *pn* junction, and in heavily irradiated detectors, the injected carriers will be trapped by the deep levels, as in the polarisation of the detector (Section 4.3.2). Under this condition, the electric field extends through the entire detector thickness, and the detector is fully depleted regardless of the voltage applied or the concentration of deep levels. For heavily irradiated detectors, the charge collection efficiency of CID is about three times higher compared to normally operated detector, thus the CID is a serious candidate to be used in the innermost parts of the tracker systems in future LHC upgrades.

The previous *IV* measurements were performed at least 30 min after irradiation, but unexpected problems occurred in the measurements of *CV* and *IV* characteristics when measurements were performed immediately after irradiation. The origin of the cause was traced to activation. In Article **III**, the Si-detectors attached to the PCB-pad were irradiated with 7 and 9 MeV protons, and the evolutions

of the *IV* and *CV* curves were measured after the irradiations. The following reactions, which induce dominant interference in the *IV* and *CV* measurements, the ^{30}Si(p,n)^{30}P in the silicon and the ^{63}Cu(p,n)^{63}Zn in the copper electrodes of the PCB, occurred. Both radionuclides are positron emitters, which generate *electron-hole* pairs in the detector, thereby increasing the reverse current. At the same time, the generated holes charge the oxide on the detector surface, thereby leading to the possible breakdown of the detector. The observed time-dependent characteristics were verified in Article **III** by modelling the activation of the detector structure.

In the above-mentioned activation studies, the positron-induced breakdown was observed for the detector structure with one guard ring, and when the detectors with a multi-guard ring structure were irradiated with applied bias voltage, we noted the proton-induced breakdown. In Article **IV**, the biased Si-detectors were irradiated with 7 and 9 MeV protons beginning with low irradiation flux and increased until the detector breaks down. The breakdown was believed to be the result of a buildup of oxide charge and was noted to depend on the flux and fluence of irradiation. Furthermore, a response function (i.e., the conversion of ionising energy loss to the production of EHP) of the Si-detectors was measured with a high particle rate being about 80%. For comparison, the response function is about 100% for single events.

Usually, the detectors are irradiated without the bias voltage, and only a few previous studies may be found [54, 55], in which the detector remained in operational mode. In Article **V**, the Si-detectors were irradiated with 7 MeV protons at 220 K. Half of the detectors were biased during irradiation, and thus a low irradiation flux was used to avoid electrical breakdown. As a result, both the introduction of a negative space charge and the irradiation-induced bulk current were about 20% lower for the detectors with simultaneously applied bias voltage than for unbiased detectors.

In all previous studies in this work, the irradiation energy was maintained high enough to penetrate protons through the detectors. This limiting energy for the detectors with a thickness of 300 μm is about 6.2 MeV (Fig. 8). For 7-MeV protons, the remaining energy after passing through the detector is about 2.8 MeV, and the corresponding value for 9-MeV protons is 6 MeV. In Article **VI**, the Si-detectors were irradiated with protons using energies between 2 MeV and 5 MeV, corresponding to ranges of 48 μm and 215 μm. As a result, the type (*n* or *p*) of defect was observed by *CV* measurements to depend on the energy: *n*-type defects are dominant for proton energies less than 1.7 MeV, and *p*-type defects are dominant for higher energies. In addition, the current-related damage [Eq. (11)] follows the NIEL scaling hypothesis for energies over 1.7 MeV, but at lower values, the damage rate is clearly lower than assumed. Consequently, the NIEL scaling is valid for proton energies above 6.5 MeV corresponding to the remaining energy of over 1.7 when the protons have passed through the 300 μm thick detector.

6 CONCLUSIONS

The irradiation facilities purposing the electrical characterisation of the silicon particle detectors were constructed in this thesis by employing a 5-MV tandem accelerator; they were then tested and proved to function well. In the near future, proton irradiations may become even more vital in developing radiation hard detectors. This is as protons create defects in silicon similar to pions, and on the other hand, MeV-proton irradiations are more efficient compared to neutron and electron irradiations. This thesis provides fundamental groundwork for MeV-proton irradiations of silicon particle detectors. Several limiting factors have resulted from material activation and irradiation-induced electrical breakdown. Moreover, the thesis takes into consideration the minimum irradiation energies at which the NIEL scaling hypothesis is valid.

It is recommended that about 15 min is waited after irradiation before starting the electrical measurements of the detectors due to activation of silicon. Clearly all materials that may become activated and lead to positron emitters with relevant half-life should be avoided in the detector concept. The activation of materials is more prominent, when the irradiation energy approaches 10 MeV (cf. Fig. 12). On the other hand, the NIEL scaling is not valid for proton energies below 1.7 MeV, thus indicating a required minimum irradiation energy of about 6.5 MeV assuming 300 μm detector thickness. Furthermore, the hardness factor is higher at lower bombarding energies leading to shorter irradiation times.

However, in order to avoid the breakdown of the detector, which is at operational mode (biased), the irradiation flux must be limited: the higher the irradiation fluence is, the lower flux is required. Fluences over 10^{14} p/cm^2 may be even unfeasible for biased detectors. In addition, the used guard ring structure and the oxide layer thickness on the detector surface affect the breakdown properties. Up to 7-MeV proton fluence of $1.25 \cdot 10^{13}$ p/cm^2 the presence of electric field decreases the introduction of negative space charge. Similarly, the reverse current is lower in case of irradiations under bias voltage.

Looking forward, the devices facilitating positron annihilation spectroscopy [Article **I**] and the microwave-probed photoconductivity transient technique (MW-PC) [9] have been installed and interrelated to the cryogenic irradiation facility. The former method provides information on vacancies, while the latter is used to determine excess charge carrier distributions. Thus far, these methods have not been intensively used in radiation hardness studies of silicon particle detectors. In the near future, emphasis will focus on extensive application of these novel facilities. In addition, in-depth studies of the irradiation of detectors (including CID) kept in operational mode at wide temperatures are of particular interest.

ACKNOWLEDGMENTS

I am most grateful to my supervisor Professor Jyrki Räisänen, the head of the Division of Materials Physics, for placing the facilities at my disposal, as well as for his kind advice and help during this work. Thank you for your never-ending encouragement and optimism. I wish to thank Professor Juhani Keinonen for giving me the opportunity to work in the field of silicon particle detectors at the Department of Physics.

I am also dearly indebted to Docent Eero Rauhala, the former head of the then Accelerator Laboratory, for drawing me to accelerator physics and for keeping me good company at lunchtime. Thanks also to my colleagues and the laboratory personnel and especially to Docent Pertti Tikkanen for his professional guidance, as well as to skilful technicians Mr Mauri Kurki, Mr Sakari Sariola, and Mr Pasi Siiki for their realisation of my ambitious plans. Mr Raimo Ingren and Mr Pietari Kienanen, the operators of the accelerator, also deserve my special thanks.

I wish to thank Docent Ivan Kassamakov, Dr Jaakko Härkönen, Dr Eija Tuominen, and all my co-authors for their fruitful co-operation. Working with you has been very pleasant. The Helsinki Institute of Physics is also acknowledged for placing their facility at my disposal.

My warmest thanks are due to my family and friends for supporting me all these years. Above all, I would like to thank my wife, Sanna, for her lovely presence during this work. My little children played a special role in reminding me of the true priorities of life.

The financial support of the National Graduate School in Materials Physics, the Magnus Ehrnrooth Foundation, and of the Väisälä Fund are gratefully acknowledged.

Helsinki, April, 2010
Samuli Väyrynen

References

[1] B. G. Streetman and S. Banerjee, *Solid State Electronic Devices*, 5th ed. (Prentice Hall, Inc, New Jersey, 2000).

[2] C. D. Via and S. J. Watts, *Can silicon operate beyond 10^{15} neutrons cm^{-2}?*, Nucl. Instrum. Methods Phys. Res. A **501**, 138 (2003).

[3] F. Gianotti *et al.*, *Physics potential and experimental challenges of the LHC luminosity upgrade*, Eur. Phys. J. C **39**, 293 (2005).

[4] C. Da Via, G. Anelli, J. Hasi, P. Jarron, C. Kenney, A. Kok, S. Parker, E. Perozziello, and S. J. Watts, *Advances in silicon detectors for particle tracking in extreme radiation environments*, Nucl. Instrum. Methods Phys. Res. A **509**, 86 (2003).

[5] G. Lutz, *Semiconductor Radiation Detectors* (Springer, Berlin, 2001).

[6] Z. Li, H. Kraner, E. Verbitskaya, V. Eremin, A. Ivanov, M. Rattaggi, P. Rancoita, F. Rubinelli, S. Fonash, C. Dale, and P. Marshall, *Investigation of the oxygen-vacancy (A-center) defect complex profile in neutron irradiated high resistivity silicon junction particle detectors*, IEEE Transactions on Nuclear Science **39**, 1730 (1992).

[7] V. Eremin, A. Ivanov, E. Verbitskaya, Z. Li, and H. Kraner, *Elevated temperature annealing of the neutron induced reverse current and corresponding defect levels in low and high resistivity silicon detectors*, IEEE Transactions on Nuclear Science **42**, 387 (1995).

[8] X. Rouby, P. Anbinderis, T. Anbinderis, J. Härkönen, P. Luukka, P. Pusa, J. Räisänen, E. Tuominen, E. Tuovinen, and S. Väyrynen, *Recent developments of CERN RD39 cryogenic tracking detectors collaboration: CERN RD39 Collaboration*, Nucl. Instrum. Methods Phys. Res. A **583**, 99 (2007).

[9] J. Višniakov, E. Gaubas, T. Čeponis, A. Uleckas, J. Räisänen, and S. Väyrynen, *Comparative investigations of recombination characteristics in proton and electron irradiated Si structures*, Lithuanian Journal of Physics **48**, 137 (2008).

[10] E. Tuominen *et al.*, *Recent progress in CERN RD39: Radiation hard cruogenic silicon detectors for applications in LHC experiments and their future upgrades*, IEEE Transactions on nuclear science **56**, 2119 (2009).

[11] J. Härkönen *et al.*, *Development of cryogenic tracking detectors for very high luminosity experiments*, Nucl. Instrum. Methods Phys. Res. A **607**, 41 (2009).

[12] S. M. Sze, *Semiconductor Devices* (John Wiley & Sons, New York, 1985).

[13] G. F. Knoll, *Radiation Detection and Measurement* (John Wiley & Sons, New York, 1989).

[14] J. von Borany, D. Beyer, V. Beyer, B. Schmidt, and B. Schnabel, *A novel silicon detector for energetic electrons with improved linearity characteristics*, Microelectronic Engineering **67-68**, 140 (2003).

[15] L. Beattie, A. Chilingarov, P. Ratoff, and T. Sloan, *Dependence of depletion Voltage and Capacitance on Temperature and Frequency in Heavily Irradiated Silicon Diodes*, ROSE Technical Note 97/4 (1997).

[16] F. Lehner, *New leakage current, noise and depletion voltage expectations for Run IIb*, DØ note 3939 draft 2.0 (2002).

[17] W. Fulop, *Calculation of avalanche breakdown voltages of silicon p-n junctions*, Solid-State Electronics **10**, 39 (1967).

[18] V. Anantharam and K. N. Bhat, *Analytical Solutions for the Breakdown Voltages of Punched-Through Diodes Having Curve Junction Boundaries at the Edges*, IEEE Transactions on electron devices **27**, 939 (1980).

[19] E. Tuovinen, *Prosessing of radiation hard particle detectors on czochralski silicon*, Ph.D. thesis, Helsinki institute of physics, P.O.Box 64, FI-00014 University of Helsinki, Finland, 2008, hIP-2008-07.

[20] J. Härkönen, E. Tuovinen, P. Luukka, E. Tuominen, Z. Li, A. Ivanov, E. Verbitskaya, V. Eremin, A. Pirojenko, I. Riihimaki, and A. Virtanen, *Particle detectors made of high-resistivity Czochralski silicon*, Nucl. Instrum. Methods Phys. Res. A **541**, 202 (2005).

[21] E. Rauhala, in *Handbook of Modern Ion Beam Analysis*, edited by J. R. Tesmer and M. Nastasi (Materials Research Society, Pittsburgh, 1995), Chap. Energy Loss.

[22] J. Ziegler, *The Stopping and Range of Ions in Matter*, , http://www.srim.org/.

[23] E. Holmström, A. Kuronen, and K. Nordlund, *Threshold defect production in silicon determined by density functional theory molecular dynamics simulations*, Phys. Rev. B **78**, 045202 (2008).

[24] J. A. Leavitt and L. C. McIntyre Jr., in *Handbook of Modern Ion Beam Analysis*, edited by J. R. Tesmer and M. Nastasi (Materials Research Society, Pittsburgh, 1995), Chap. Backscattering Spectrometry.

[25] V. Markevich, A. R. Peaker, and A. N. Larsen, in *Germanium-Based Technologies*, edited by C. Clayes and E. Simoen (Elsevier, Amsterdam, 2007), Chap. Radiation Performance of Ge Technologies.

[26] S. Mäkinen, H. Rajainmäki, and S. Linderoth, *Low-temperature positron-lifetime studies of proton-irradiated silicon*, Phys. Rev. B **42**, 11166 (1990).

[27] A. Holmes-Siedle and L. Adams, *Handbook of radiation effects* (Oxford Universituy Press, Oxford, 2000).

[28] D. Pitzl, N. Cartiglia, B. Hubbard, D. Hutchinson, J. Leslie, K. O'Shaughnessy, W. Rowe, H. F. W. Sadrozinski, A. Seiden, E. Spencer, H. J. Ziock, P. Ferguson, K. Holzscheiter, and W. F. Sommer, *Type inversion in silicon detectors*, Nucl. Instrum. Methods Phys. Res. A **311**, 98 (1992).

[29] Z. Li, M. Bruzzi, V. Eremin, J. Harkonen, J. Kierstead, P. Luukka, D. Menichelli, Tuominen, E. Tuovinen, and E. Verbitskaya, *Gamma radiation induced space charge sign inversion and re-inversion in p-type MCZ Si detectors and in proton-irradiated n-type MCZ Si detectors*, Nucl. Instrum. Methods Phys. Res. A **552**, 34 (2005).

[30] K. Leinonen, T. Palviainen, T. Tuuva, E. Tuovinen, J. Härkönen, and P. Luukka, *Investigation of type inversion of n-bulk in 10 MeV proton-irradiated FZ silicon detectors using a scanning electron microscope*, Nucl. Instrum. Methods Phys. Res. A **552**, 357 (2005).

[31] N. Manna, D. Bassignana, M. Boscardin, L. Borrello, M. Bruzzi, D. Creanza, M. de Palma, V. Eremin, A. Macchiolo, D. Menichelli, A. Messineo, V. Radicci, M. Scaringella, and E. Verbiskaya, *Space charge sign inversion investigation in n-type MCz silicon diodes irradiated by 24 GeV/c and protons and reactor neutrons*, Nucl. Instrum. Methods Phys. Res. A **583**, 87 (2007).

[32] J. Matheson, M. Robbins, S. Watts, G. Hall, and B. MacEvoy, *A microscopic explanation for type inversion and the annealing behaviour of radiation damaged silicon detectors*, Nucl. Instrum. Methods Phys. Res. A **371**, 575 (1996).

[33] E. Borchi, M. Bruzzi, S. Pirollo, and S. Sciortino, *Temperature and frequency dependence of the capacitance of heavily irradiated silicon diodes*, Solid-State Electronics **42**, 2093 (1998).

[34] G. Lindström, *Radiation damage in silicon detectors*, Nucl. Instrum. Methods Phys. Res. A **512**, 30 (2003).

[35] M. Huhtinen, *Simulation of non-ionising energy loss and defect formation in silicon*, Nucl. Instrum. Methods Phys. Res. A **491**, 194 (2002).

[36] G. Lindström *et al.*, *Developments for radiation hard silicon detectors by defect engineering–results by the CERN RD48 (ROSE) Collaboration*, Nucl. Instrum. Methods Phys. Res. A **465**, 60 (2001).

[37] A. Vasilescu and G. Lindström, *Displacement damage in silicon, on-line compilation*, , http://sesam.desy.de/members/gunnar/Si-dfuncs.html.

[38] R. Wunstorf, H. Feick, E. Fretwurst, G. Lindström, G. Lutz, C. Osius, R. Richter, T. Rohe, A. Rolf, and P. Schlichthärle, *Damage-induced surface effects in silicon detectors*, Nucl. Instrum. Methods Phys. Res. A **377**, 290 (1996).

[39] G. Lutz, *Radiation Damage in Structured Silicon Semiconductor Detectors*, , MPI-report:MPI-PhE/2002-21, 2002.

[40] R. Parizotto and H. Boudinov, *Irradiation effects of proton bombarded poly-Si/SiO_2/Si structure*, Nucl. Instrum. Methods Phys. Res. B **218**, 262 (2004).

[41] B. Dezillie, V. Eremin, Z. Li, and E. Verbitskaya, *Polarization of silicon detectors by minimum ionizing particles*, Nucl. Instrum. Methods Phys. Res. A **452**, 440 (2000).

[42] G. Pfennig, H. Klewe-Nebenius, and W. Seelmann-Eggebert, *Karlsruher Nuklidkarte* (Forschungszentrum Karlsruhe Gmbh, Karlsruhe, 1998).

[43] *National nuclear data center*, , http://www.nndc.bnl.gov/.

[44] N.Yamano, *Table of Isotope Production Cross Sections*, , http://wwwndc.jaea.go.jp/ftpnd/sae/acl.html.

[45] P. Tikkanen, V. Palonen, H. Jungner, and J. Keinonen, *AMS facility at University of Helsinki*, Nucl. Instrum. Methods Phys. Res. B **223-224**, 35 (2004).

[46] V. Palonen, P. Tikkanen, and J. Keinonen, *Ion optical modelling of the Helsinki AMS system*, Nucl. Instrum. Methods Phys. Res. B **223-224**, 227 (2004).

[47] M. Moll, E. Fretwurst, G. Lindström, and ROSE/CERN-RD48 collaboration, *Leakage current of hadron irradiated silicon detectors Ð material dependence*, Nucl. Instrum. Methods Phys. Res. A **426**, 87 (1999).

[48] K. Arndt, G. Bolla, D. Bortoletto, K. Giolo, R. Horisberger, A. Roy, T. Rohe, and S. Son, *Silicon sensors development for the CMS pixel system*, Nucl. Instrum. Methods Phys. Res. A **511**, 106 (2003).

[49] V. Eremin, N. Strokan, E. Verbitskaya, and Z. Li, *Development of transient current and charge techniques for the measurement of effective net concentration of ionized charges (N_{eff}) in the space charge region of p-n junction detectors*, Nucl. Instrum. Methods Phys. Res. A **372**, 388 (1996).

[50] A. Castaldini, A. Cavallini, L. Polenta, F. Nava, and C. Canali, *Electric field distribution in irradiated silicon detectors*, Nucl. Instrum. Methods Phys. Res. A **476**, 550 (2002).

[51] Cremat, Inc, *Detection electronics by Cremat, Inc*, , http://www.cremat.com/.

[52] Tektronix, *TDS1000B/2000B Oscilloscope Series*, , http://www.tek.com/products/oscilloscopes/tds1000_tds2000/.

[53] L. Beattie, A. Chilingarov, and T. Sloan, *Forward-bias operation of Si detectors: a way to work in high-radiation environment*, Nucl. Instrum. Methods Phys. Res. A **439**, 293 (2000).

[54] V. Cindro, G. Kramberger, M. Mikuž, and D. Žontar, *Bias-dependent annealing of radiation damage in neutron-irradiated silicon p^+-n-n^+ diodes*, Nucl. Instrum. Methods Phys. Res. A **419**, 132 (1998).

[55] V. Cindro, G. Kramberger, M. Mikuž, M. Tadel, and D. Žontar, *Bias-dependent radiation damage in high-resistivity silicon diodes irradiated with heavy charged particles*, Nucl. Instrum. Methods Phys. Res. A **450**, 288 (2000).